ASME paper 99-GT-146, ASME Turbo Expo, Indianapolis, IN, June 7-10, 1999

MINIMIZATION OF COOLANT MASS FLOW RATE IN INTERNALLY COOLED GAS TURBINE BLADES

Thomas J. Martin[+], George S. Dulikravich[++], Zhen-Xue Han[*], Brian H. Dennis[**]
The Pennsylvania State University, Department of Aerospace Engineering
University Park, PA 16802

All correspondence should be addressed to:
Dr. George S. Dulikravich
The Pennsylvania State University
Department of Aerospace Eng., 233 Hammond
University Park, PA 16802
phone: (814) 863-0134 fax: (814) 865-7092 e-mail:ft7@psu.edu

[+]Currently with Federal Data Corp., NASA Langley Research Center, Hampton, VA. Associate member ASME.
[++]Associate Professor. Fellow ASME.
[*]Visiting Scholar, BUAA, Beijing, China.
[**]Graduate Research Assistant. Student member ASME.

ABSTRACT

This paper presents a coupled aerodynamic and thermal study of computer-automated design and optimization of internally cooled turbine blades. The turbine blade, thermal barrier coating, coolant passages, and struts were developed from a set of design variables, including β-splines for the coolant wall thickness distribution. The turbine inlet temperature, mass flow rate, and coolant wall roughness were also incorporated into the design variable set. The maximum temperature in the metal blade was enforced with equality or inequality constraint functions. Because the coolant flow rate was a design variable, this function could not be explicitly minimized. Instead, three different thermal objective functions were studied: uniform temperature, heat flux extremum, and minimum coolant ejection temperature. A constrained hybrid optimization algorithm was developed and used to modify the turbine blade designs until an optimum design was found. This evolutionary optimization package incorporated four popular algorithms (steepest descent, genetic, simplex, and simulated annealing) with automatic switching among them. A heat conduction analysis, using the boundary element method (BEM), was iteratively coupled to an unstructured finite volume Reynolds-averaged Navier-Stokes CFD analysis for turbulent hot gas flow. A quasi-one-dimensional system with heat addition and friction was iteratively coupled to the BEM heat conduction via heat flux for the simulation of the airflow in the serpentine coolant passages. This quasi-one-dimensional system yielded correlations for the heat convection coefficients on the coolant passage walls. The coolant passage pressure loss was one of the quantities arising from the quasi-one-dimensional analysis. Results have shown that it is possible to increase or maintain high turbine inlet temperatures while decreasing the turbine blade coolant requirements.

NOMENCLATURE

A	Cross sectional area of a coolant passage
c_p, c_v	Specific heats of coolant fluid
D_h	Hydraulic diameter of a coolant passage
e_S	Strut filleting super-elliptic exponent
ε	Coolant passage wall roughness
f	Friction factor
F	Optimization objective function
Φ	Viscous dissipation function
$\gamma = c_p/c_v$	Ratio of specific heats
h_{cool}	Heat transfer coefficient on coolant channel walls
h_O	Heat transfer coefficient on outer turbine airfoil surface
k	Thermal conductivity coefficient
$\dot{m}$	Mass flow rate of coolant fluid
μ	Coolant fluid viscosity coefficient
N_{strut}	Number of struts
ρ	Density of coolant fluid
s	Turbine airfoil contour following coordinate
p_{cool}	Coolant fluid inlet pressure
p_{eject}	Coolant fluid trailing edge ejection pressure
Q	Heat flux
R	Specific gas constant
R_K	Coolant pressure loss coefficient in a 180° turning bend
t_S	Strut thickness

T	Temperature
T_{cool}	Bulk temperature of coolant
T_{eject}	Coolant fluid ejection temperature
T_{inlet}	Turbine inlet temperature
T_{max}	Maximum temperature in turbine blade metal
$\overline{T}$	Mean or target temperature
τ_w	Coolant fluid wall shear stress
V	Vector of optimization design variables
w	Coolant fluid average local speed
W	Coolant passage wall thickness
xs	Coordinate of strut centerline intersection with turbine airfoil
x,y	Local coordinate system in plane of turbine airfoil
z	Streamwise direction of coolant flow

1. INTRODUCTION

The maximum temperature within a turbine blade must be maintained below a certain value in order to avoid thermal creep, melting, and oxidation problems. Internal cooling schemes of modern turbojet and turbofan engines bleed air from the compressor and pass this air into the serpentine coolant flow passages within the turbine blades. With the exception of film cooling, the temperature in the turbine blade is reduced primarily because of convection cooling on the internal coolant passage walls. The use of mechanical turbulators like boundary layer trip strips result in high pressure losses in the coolant passages, thus requiring the coolant air to be bled from higher pressure compressor stages. Increased coolant heat transfer and increased coolant flow rate directly decrease the amount of air delivered to the combustor and increase specific fuel consumption.

This paper introduces a multi-disciplinary optimization program that computer-automates the process of turbine blade internal cooling scheme design. Using this approach, realistic geometric models for

internal coolant flow passages were developed automatically, without user intervention, from a set of approximately 30 design variables. These design variables defined the coolant passage configuration, variable passage wall roughness, coolant mass flow rate, and turbine inlet temperature. A hybrid numerical optimization program then iteratively modified sequential sets of these design variables in order to achieve internal cooling configurations that require a lesser amount of coolant air flow. Turbine blade integrity and high turbine inlet temperatures were maintained by constraining the maximum temperature in the turbine blade. This multi-disciplinary design tool used fully-coupled two-dimensional aero-thermal numerical analysis programs for the turbulent transonic turbine cascade flow-field analysis and blade heat conduction. Forced convection correlations were used to obtain heat transfer coefficients on the walls of the internal coolant flow passages. The bulk temperatures and pressure losses in the coolant passages were computed from a quasi-one-dimensional system that modeled the air flow in the serpentine coolant passages. The presented test cases demonstrate the main features of the design system.

1.1 Geometry Model of the Turbine Blade Coating and Coolant Flow Passages

The blade outer shape was assumed as already determined by aerodynamic inverse shape design or optimization and was kept fixed during the entire thermal optimization procedure.

Specifying its thickness inward to the outer airfoil surface created a thermal barrier coating. The coating thickness was described by a wall thickness function versus the airfoil contour following coordinate, s. The first step in the development of the multiple coolant flow passages was the description of the cooling wall thickness function. The wall thickness function's ordinate, W(s), determined the thickness of the wall between the hot gas and coolant fluid. The abscissa followed counter-clockwise along the metal/coating interface, s, all the way around the airfoil, from trailing edge to trailing edge, and formed a closed loop. It is shown in Figure 1, where the local coordinate system (x,y) was fixed upon a curved surface at a constant radius from the engine axis. W(s) was defined by a piecewise-continuous β-spline (Barsky, 1988) curve that varied in the direction normal to the

metal/coating interface to a distance controlled by one design variable per β-spline control vertex (Martin and Dulikravich, 1997; Dulikravich et al. 1998a; 1998b). For this manuscript, the number of coolant flow passages in the turbine blade, $N_{hole} = N_{strut} + 1$, was kept fixed. The computational domain was divided into a finite number of sub-domains where the material properties within each sub-domain varied continuously, homogeneously, and isotropically.

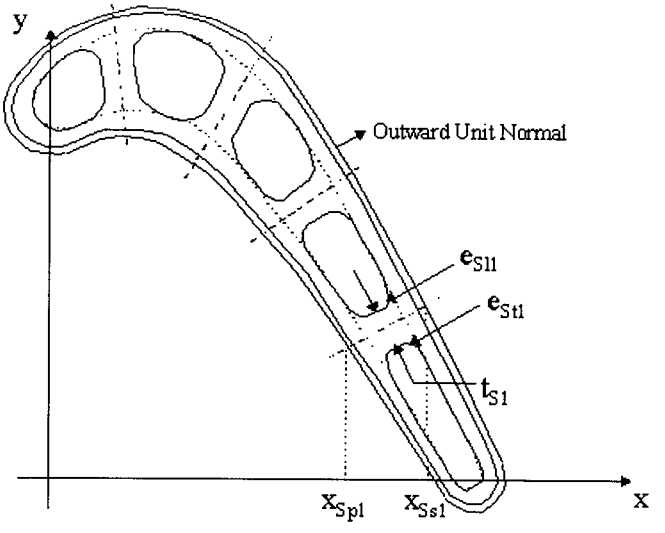

Figure 1. Turbine airfoil, coating and coolant passage geometry. The outer turbine blade surface and coating/metal interface are shown as solid lines. The cooling wall thickness function is used as a reference (dotted line) to draw the coolant passage walls (solid lines).

Next came the specification of the locations of the strut centerlines.

The x-coordinates of the intersections of the strut centerlines with the outer turbine airfoil shape were defined as x_{Ssi} and x_{Spi}, for the suction and pressure sides of the blade, respectively. The index i varied from 1 to the number of struts, N_{strut}. The range over which each strut could vary was $\pm\Delta x_{Si}$. In addition to the coordinates of the strut intersections, the strut thickness, t_{Si}, and a filleting exponent on either the trailing or leading edge sides, e_{Sti} and e_{Sli}, respectively, were used to complete the geometric

modeling of each strut. The strut fillets were described by a super-elliptic function that varied from a circular fillet ($e_{Si} = 2$) to an almost sharp right angle ($e_{si} \rightarrow \infty$).

2. HEAT CONDUCTION

The conduction of heat within the solid turbine blade was modeled by the following steady-state non-linear partial differential equation.

$$\nabla \bullet (k_m(T)\nabla T) = 0 \qquad (1)$$

The thermal conductivity coefficient in the mth sub-domain was assumed to be a function of temperature, that is, $k_m(T)$. When the coefficient of thermal conductivity was temperature-dependent, the heat conduction equation was linearized by the application of Kirchhoff's transformation (Arpaci, 1966). The steady-state heat conduction equation (1) was numerically evaluated with the Boundary Element Method (BEM) (Brebbia, 1978). The advantages of the BEM are realized whenever linear boundary value problems are solved. It eliminates the need for the often-difficult task of generating an internal boundary-conforming computational grid in a multiply connected domain. In the case of inverse shape design problems, where the geometry changes iteratively many times during the solution process, this benefit provides substantial savings in computer resources. Also, the temperature gradients computed by the BEM are of the same order of accuracy as the predicted temperatures. Therefore, BEM predicts heat fluxes more accurately than when using finite elements or finite difference methods, on the same grid.

3. HEAT CONVECTION

In the thermal shape optimization problem, the outer surface of the turbine blade was subject to forced convection heating.

$$Q = -k\frac{\partial T}{\partial n} = h_0(T - T_{inlet}) \qquad (2)$$

Here, h_O is the convection heat transfer coefficient that varied along the surface of the turbine airfoil, and T_{inlet} is the turbine inlet static temperature. This temperature was used as a design variable in the numerical optimization procedure. The variation of the heat transfer coefficient on the outer surface of the turbine blade was obtained from a computational thermal-fluid dynamics analysis where the following heat flux compatibility equation was used on the surface exposed to the hot combustion product gases.

$$-k_S\left(\frac{\partial T}{\partial n}\right)_S = k_F\left(\frac{\partial T}{\partial n}\right)_F \qquad (3)$$

Here, k_S is the thermal conductivity of the most outer solid sub-domain (coating) and k_F refers to the thermal conductivity of external combustion product gases. An iterative coupling of the boundary conditions between the BEM heat conduction program and the finite volume CFD program provided a scheme for conjugate heat transfer. It required only a small number of iterations (1-8) between the two programs (He, Kassab, Bishop, and Minardi, 1995).

3.1 Forced Convection Correlations for Internal Coolant Passage Heat Transfer

The internal coolant flow within modern gas turbine blade coolant passages is extremely complex and three-dimensional, having recirculating flows caused by the existence of miniature heat exchangers, skewed trip strips, bifurcations of the flow stream, 180-degree bends, pedestal cooling schemes, leading

edge impingement schemes, and film cooling passages. The complexity of the CFD computation becomes even greater because of the contribution of thermal buoyancy. Coriolis forces affect each portion of the serpentine coolant passages differently depending upon whether the coolant stream is traveling radially-outward or radially-inward (Mochizuki et al., 1994). At present, the computational requirements needed for this type of analysis are still too costly for fully three-dimensional numerical optimization purposes (Stephens and Shih, 1997). Therefore, a fully three-dimensional conjugate coupling of the coolant flow is, for now, beyond the scope of this paper.

Instead, the application of thermal boundary conditions on the internal coolant flow passage surfaces was greatly simplified by the specification of convective heat transfer coefficients and bulk fluid temperatures of the coolant fluid. Semi-empirical correlations were used to determine the coolant heat transfer coefficients, $h_{cool,n}$, and the bulk coolant temperatures, $T_{cool,n}$, for each nth coolant passage. They were assumed to vary only in the radial direction (from the root to tip sections) and among the coolant passages.

Appropriate to the physical phenomenon of forced convection, the heat transfer coefficient, h_{cool} should be allowed to vary with the following parameters: w, ρ, D_h, T, T_{cool}, ε, temperature-dependency of the fluid properties, μ, k, c_p, the thermal buoyancy, and the geometric shape. This variation can be expressed functionally (White, 1988, Chapter 5). Assumptions have been made in order to simplify this functional and to arrive at a usable relationship. Specifically, the temperature differences were small, thus allowing elimination of the temperature-dependency of physical properties. Also, thermal buoyancy, centripetal, and Coriolis forces were neglected.

Because turbine blade internal coolant passages do not, in general, have circular cross sections, the heat transfer correlations were based on the hydraulic diameter of the coolant passages, $D_h = 4A/P$, where P was the wetted perimeter of the nth coolant flow passage.

The coolant mass flow rate, $\dot{m} = \rho A w$, was specified as a boundary condition. It was often the most important design variable during the optimization process. The coolant flow rate could not be explicitly

minimized, because of its independence as a boundary condition. This will be discussed in greater detail later in the paper.

Modern internal cooling designs utilize boundary layer trips in order to increase the heat transfer coefficients. They induce early transition to turbulence and greatly increase the channel friction, while moderately increasing the convective heat transfer (White, 1974). Results of experimental data correlations for rough tubes, such as those containing trip strips, are rather sparse. The effect of placing trip strips in the coolant passages was, therefore, simulated with large wall roughness values as design variables. The Reynolds analogy provided a relationship between the wall shear stress and the heat transfer.

$$St = \frac{f/8}{1+12.7\left(Pr^{2/3}-1\right)\sqrt{f/8}} \qquad (4)$$

Here, the Stanton number, $St = h_{cool}/\rho c_p w$, the Prandtl number, $Pr = \mu c_p/k$, and the friction factor, $f = 8\tau_w/\rho w^2$, were based on the bulk properties of the coolant fluid. The value of the friction factor was taken from the Moody chart knowing the relative roughness ratio, ε/D_h, and the Reynolds number (Holman, 1981, pp. 230). For optimization purposes, the friction factor will change during the numerical optimization process. Therefore, an explicit formula given by Haaland was used (White, 1994, pg. 317).

$$\frac{1}{\sqrt{f}} = -1.8\log\left[\frac{6.9}{Re_D}+\left(\frac{\varepsilon/D_h}{3.7}\right)^{1.11}\right] \qquad (5)$$

This explicit expression is accurate to within 2% of the Moody chart, which itself is accurate to +/-15% versus experimental data for fully turbulent flows having Reynolds numbers in the range $10^3 < Re < 10^8$. During the numerical optimization procedure, the relative wall roughness heights of each coolant

passage were independent design variables ranging from $\varepsilon/D = 0$ up to a user-specified limit, usually $\varepsilon/D = 0.1 - 0.2$.

The coolant streamwise pressure gradients, $(dp/dz)_n$, were used to determine the minimum required compressor air bleed pressure. That is, the static pressure, p_{cool}, at the inlet of the coolant flow passage (root of leading edge passage) was determined given the knowledge of a fixed static pressure, p_{eject}, at the exit of the coolant flow passages (trailing edge ejection) and the pressure losses in the coolant passages.

$$p_{cool} = p_{eject} - \sum_{n=1}^{Ncool} \left(\frac{dp}{dz}\right)_n \Delta z_n \qquad (6)$$

The trailing edge ejection static pressure was either computed by a CFD prediction of the turbulent transonic flow through the turbine cascade (in the case of trailing edge coolant ejection) or it was specified as a design condition (in the case of a closed loop cooling systems). The resulting inlet coolant static pressure, p_{cool}, was a function of the coolant mass flow rate, the relative wall roughness, the inlet coolant air pressure, the material properties, coolant passage geometry, and the heat flux into the turbine blade numerically predicted by the BEM.

Most internal cooling schemes have serpentine passages that cause the coolant to undergo sharp turnings so that it can flow outward towards the tip of the blade and inward towards the root of the blade several times. Therefore, the equation for trailing edge ejection pressure also included the pressure losses associated with 180° flow turns (White, 1988),

$$\Delta p_{turn} = \frac{1}{2}\rho w^2 R_K \qquad R_K = \frac{0.4}{(36.37 D_h)^{0.2}} \qquad (7)$$

where the hydraulic diameter, D_h, is in meters.

The temperature of the coolant at the inlet of the passages was determined given the fact that the turbine coolant fluid was derived from air bled from the compressor. The adiabatic compression heating equation was used for the relationship between inlet coolant static temperature, T_{cool}, and the static pressure, p_{cool}. With the perfect gas assumption, the following equation for inlet coolant temperature provided an inlet coolant passage boundary condition.

$$\frac{p}{\rho^{\gamma}} = p^{1-\gamma} R^{\gamma} T^{\gamma} = \text{constant} \qquad (8)$$

The inlet coolant conditions were related to the atmospheric pressure, p_{atm}, and temperature, T_{atm}, by this equation.

3.2 Quasi-One-Dimensional Coolant Flow with Heat Addition and Friction

The steady state, quasi-one-dimensional compressible system of Navier-Stokes equations was used to determine the bulk temperatures within the serpentine coolant channels. The coolant flow direction, z, began at the coolant flow inlet at the root of the leading edge passage, followed along the length of each coolant passage in the serpentine, past 180 degree turning bends around the struts, and finally ending at the trailing edge ejection slot. The following three ordinary differential equations were used in conjunction with the ideal gas equation of state to solve for the four unknown primitive variables: coolant air density $\rho = \rho(z)$, average coolant speed $w = w(z)$, coolant static pressure $p = p(z)$, and coolant static temperature $T = T(z)$.

Continuity $$\frac{d}{dz}(\rho w A) = 0 \qquad (9)$$

Linear momentum

$$\frac{d}{dz}\left(\rho\frac{w^2}{2}A + pA\right) = -\frac{4A}{D_h}\tau_w - R_K\left(\rho\frac{w^2}{2}\right)\frac{A}{L} \qquad (10)$$

Energy $$\frac{d}{dz}\left(c_pT + \frac{w^2}{2}\right) = \frac{Q+\Phi}{\dot{m}} \qquad (11)$$

In these equations; z is the streamwise direction of the coolant flow with L being the length of the passage in that direction, $\tau_w = \tau_w(z)$ is the shear stress on the walls of the coolant passage, A = A(z) is the cross-sectional area of the coolant passage, Q = Q(z) is the heat flux per unit area into the coolant predicted by the BEM, $\Phi = \Phi(z)$ is the viscous dissipation function, and $R = c_p - c_v$ is the specific gas constant. The wall shear stress was taken from empirical correlations presented in the previous section. The viscous dissipation function was derived from the wall shear stress and the 180° turning bend losses.

$$\Phi = \frac{4A}{D_h}\tau_w w + R_K\left(\rho\frac{w^2}{2}\right)\frac{A}{L}w \qquad (12)$$

Given the fact that the mass flow rate was constant along the entire length of the coolant channel (no film cooling), the energy equation was recast into total enthalpy conservation form.

The entire serpentine coolant flow passage was discretized into a total of K cells in series. In the two-dimensional problem, the radial dimension and the z direction were parallel and constant. Only the average blade length from the root to tip ($L = z_{blade}$) was required. For an incompressible coolant, only $K = N_{cool}$ cells were needed, one for each coolant flow passage. In the three-dimensional problem, the coolant passage cross-sectional area, as well as the primitive variables and most of the heat transfer parameters, varied in the radial direction. The blade length from the root to tip was discretized into a total of k_{cell} cells.

An iterative strategy was used to converge on the non-linearity and the sweeping direction was based upon the propagation of boundary condition information in the coolant flow (z) direction. Three boundary conditions were applied: coolant static pressure at the trailing edge ejection, coolant adiabatic heating equation, and the coolant mass flow rate. The following procedure was used to numerically solve the quasi-one-dimensional system (equations 9-11).

1. Specify and initial conditions for the primitive variables.
2. Compute the spanwise derivatives (d/dz) of the primitive variables.
3. Sweep upstream from the trailing edge ejection slot and determine the static pressures, p(z), having knowledge of p_{eject} and $(dp/dz)_k$.
4. Use adiabatic heating equation and p_{cool} to determine the inlet coolant temperature T_{cool}.
5. Sweep downstream from the coolant passage inlet (blade leading edge root) section and determine the static coolant temperatures, T(z), using T_{cool} and $(dT/dz)_k$. Compute also the static coolant temperature at the trailing edge ejection, T_{eject}, having knowledge of the geometric shape and size of the ejection slot.
6. Use the equation of state to compute the coolant density, $\rho(z)$, in each coolant passage.
7. Given a constant coolant mass flow rate (assuming no film cooling), determine the coolant average local speed, w(z), values.
8. Update the solution vector containing the primitive variables, $\rho(z)$, w(z), p(z) and T(z), and iterate beginning with step 2 until convergence.

Because the bulk coolant temperatures, $T_{cool,n}$, were functions of the heat flux, the solution to the computational heat conduction (or conjugate) equation was non-linear due to its Robin boundary condition on the coolant passage walls. The initial heat fluxes, Q_n, into each coolant passage were set equal to the net heat flux into the turbine blade divided by the number of coolant passages. In the coupled computational aero-thermal method, the net heat flux was obtained from the CFD analysis of the hot gas flow around the turbine cascade, making the entire process fully conjugate. Subsequent solutions to the heat conduction (or conjugate solver) provided better estimates of the heat flux distributions on the

walls of the coolant passages. An iterative scheme was utilized until the computed heat fluxes converged to within a reasonable residual. This was accomplished in about 6 iterative solutions of the heat conduction analysis from the initial guess, with subsequent analyses taking only 1-3 iterations.

The heat transfer characteristics in a real rotating serpentine coolant flow passage are very complex and three-dimensional, being affected by Coriolis and centrifugal forces combined with thermal buoyancy. Hot zones have a distinct effect on the heat transfer rate because higher temperatures produce greater buoyancy forces and enhanced heat transfer. For example, when secondary flows are induced by Coriolis forces, the heat transfer coefficients in the radially outward passages diminish on the leading surface, but increase on the trailing surface with an increase in rotational speed. The trend is reversed in the radially inward passage. In order to account for the rotating serpentine flow, the Nusselt number ratios, Nu/Nu_{cool}, could be adjusted (Mochizuki, et al., 1994). Further study is needed in these areas before an empirical correlation between the heat transfer rate and rotation can be reliable within the ranges of Reynolds, Grashof, and rotation numbers encountered in a real turbine.

4. THERMAL SHAPE OPTIMIZATION

During the past fifteen years, Dulikravich and his research team of graduate students have developed a fully-automatic computational inverse shape design algorithm that allows a cooling systems designer to determine the numbers, sizes, shapes, and locations of coolant flow passages within internally cooled configurations (Dulikravich and Martin, 1996). A desirable variation of heat flux over the external surface of the turbine blade was needed in addition to the boundary conditions of a well-posed heat conduction problem. An optimization algorithm was then used to iteratively modify the shapes of the guessed coolant passages in an attempt to achieve the least square sum of the differences between the user-specified and computed heat fluxes on the blade outer boundary. The methodology was successfully demonstrated on multi-holed two-dimensional turbine airfoils with thermal barrier coatings and single-holed three-dimensional turbine blades.

Although the inverse thermal shape design problem provided a very fast and robust method of automatic coolant passage design, it lacked generality. Primarily, the engineer does not know in advance the optimal temperature and heat flux distributions on the external turbine blade surface. Specifying these variations is similar to the idea of designating a target pressure distribution on an airfoil surface for inverse aerodynamic shape design. In the same way that engineering expertise is necessary to correlate the qualitative nature of airfoil pressure distributions to their aerodynamic performance, so there must also be an understanding of the heat transfer into the turbine blade for improved durability with reduced coolant flow requirements. There has not yet been a direct correlation between a particular temperature or heat flux distribution and the coolant flow passage performance, except for the fact that enhanced heat transfer coefficients increase the convective heat transfer to the coolant.

A quantifiable objective function that assesses the performance and durability of internally cooled configurations for numerical optimization does not exist. In order to construct an effective thermal optimization strategy, three different thermal objective functions have been studied, (1) uniform blade temperature, (2) integrated surface heat flux extremization, and (3) minimum coolant ejection temperature.

4.1 Uniform Temperature Distribution

The thermal optimization strategy began with the use of an objective that closely resembled those from inverse thermal shape design. Here, the integrated difference between the computed temperature and user-specified target or mean temperature, $\overline{T}$, was minimized. The numerical optimization algorithm modified the coolant passage scheme in order to minimize the squared difference between the local computed temperature and the specified constant mean temperature. The integration was either carried out over the boundary or over the domain.

$$F(V_i) = \int_{\Gamma} (T - \overline{T})^2 \, d\Gamma \qquad F(V_i) = \int_{\Omega} (T - \overline{T})^2 \, d\Omega \qquad (13)$$

As this function was minimized, the temperature field within the turbine blade approached the desired value, reducing the temperature gradients and producing a more uniform temperature distribution. The primary benefit of this is the reduction in the thermal stresses. Domain integration has the added advantage of simultaneously minimizing weight. The iteratively updated mean temperature could also be used as an alternative to specifying a desired target temperature.

$$\overline{T} = \int_{\Gamma_o} T d\Gamma \Big/ \int_{\Gamma_o} d\Gamma \qquad (14)$$

4.2 Net Integrated Heat Flux

For minimum coolant flow rate, the thermal objective was initially formulated as the minimization of the integrated heat flux into the turbine blade. This objective concerned itself directly with the reduction of the coolant flow requirements by reducing the heat transfer absorbed by the coolant. The integration was carried out over the outer turbine airfoil boundary, Γ_O.

$$F(V_i) = -\int_{\Gamma_o} Q d\Gamma \qquad (15)$$

When increasing the turbine inlet temperature was more desirable than reducing the coolant flow requirements, the opposite objective, maximization of the net heat flux into the blade, was attempted. Obviously, an increase in turbine inlet temperature lead directly to an increase in heat flux. This was expected, because an increase in the convection heating on the outer surface of the turbine blade would require more cooling to sustain the heat loads. Investigations involving the minimum net heat flux objective have shown that, when performing the single disciplinary thermal optimization, the sizes of the coolant flow passages were reduced as much as possible. The maximum heat flux objective produced

the opposite trivial result, making the coolant walls as thin as possible. It has been concluded that these objectives are not viable strategies for the internal coolant passage optimization.

4.3 Coolant Ejection Temperature

In order to minimize the coolant flow requirements with less geometric influence, the objective was re-formulated to the minimization of the coolant ejection temperature.

$$F(\vec{V}) = T_{eject} \qquad (16)$$

4.4 Turbine Blade Integrity Constraints

The uniform temperature field objective improved the turbine blade durability, but the turbine blade integrity was maintained by ensuring that the maximum temperature within the turbine blade did not exceed its melting or oxidation temperatures. In the thermal optimization procedure, thermal integrity was strictly enforced by the following inequality constraint function.

$$g_1(V_i) = \frac{T_{max}}{\overline{\overline{T_{max}}}} - 1 < 0 \qquad (17)$$

The constrained optimization algorithm never accepted designs in which this function was violated.

Forced convective heat transfer on the surface of the turbine blade makes the maximum temperature in the solid turbine blade, T_{max}, a strong function of the turbine inlet temperature. Because we wish to maximize the turbine inlet temperature, but keep it below the limiting value at the melting point, optimum thermal durability takes the form of an equality constraint.

$$h_1(V_i) = \frac{T_{max}}{\overline{\overline{T_{max}}}} - 1 = 0 \qquad (18)$$

This constraint forces the maximum temperature in the metal blade to be equal to some percentage of its melting or oxidation temperature. Thus, for a given turbine inlet temperature, an optimal turbine cooling scheme is the one that keeps the maximum temperature in the metal blade at some limiting value with the least mass flow rate of the coolant. To look at it from the viewpoint of the constraints, for a given coolant flow rate, the turbine inlet temperature should be increased to the point where the maximum temperature of the blade reaches its material limit.

4.5 Evolutionary Hybrid Optimization Algorithm

A constrained evolutionary hybrid optimization scheme has been developed in the FORTRAN programming language. This algorithm creates N_{pop} design variable vectors, $\vec{V}$, subject to inequality and/or equality constraint functions, in addition to their lower and upper bounds, $\vec{V}_{min}$ and $\vec{V}_{max}$, respectively. Those design variables that are feasible have their objective function value, $F(\vec{V})$, evaluated and that information is saved into the population matrix, $P\{\vec{V}_1, \vec{V}_2, \ldots, \vec{V}_{Npop}\}$. The optimization program creates sequential sets of population matrices in order to minimize the objective function value and evolve the population towards the global minimum.

There are many optimization algorithms in the open literature and various ones have been shown to provide faster convergence over others depending upon the size and shape of the mathematical design space, the nature of the constraints, and where they are during the optimization process. Our hybrid optimizer incorporates four of the most popular optimization approaches; the Davidon-Fletcher-Powell (DFP) gradient search method, a genetic algorithm (GA) (Goldberg, 1989), the Nelder-Mead (NM) simplex method, and simulated annealing (SA) (Press et al., 1986). A set of rules and heuristics were developed to switch back and forth among the different optimization algorithms as the program evolved the population matrix.

The evolutionary hybrid scheme handled the existence of equality and inequality constraint functions, $g(\vec{V})$ and $h(\vec{V})$, in three ways: Rosen's projection method, feasible search, and random design generation.

Rosen's projection method (Haftka and Gurdal, 1992) provided search directions which guided the descent direction tangent to active constraint boundaries. In the feasible search (Foster and Dulikravich, 1997), designs that violate constraints were automatically restored to feasibility via the minimization of the active global constraint functions. If at any time this constraint minimization failed, random designs were generated within a Gaussian-shaped probability density cloud about a desirable and feasible design until a new design is reached.

Gradients of the thermal objective and constraint functions with respect to the design variables, $\partial F/\partial \vec{V}$, $\partial g/\partial \vec{V}$, and $\partial g/\partial \vec{V}$ also called design sensitivities, were calculated using either forward (first order) finite difference formulas, or by the much more efficient method of implicit differentiation of the governing equations (Haftka and Malkus, 1981).

The population was updated every iteration with new designs and ranked according to the value of the objective function. As the optimization process proceeded, the population evolved towards the global minimum. The optimization problem was completed when the best design in the population was equivalent to a target design or when all four optimization algorithms failed to produce a non-negligible decrease in the objective function.

5. NUMERICAL RESULTS

During the course of this research, many runs were attempted on turbine blades using the full thermal optimization procedure, sometimes on different geometries, sometimes with different boundary conditions, and other times with different target conditions. This section attempts to address the issues that were raised in the process of that work.

5.1 Turbine Cooling Scheme Optimization for Uniform Temperature

All cases discussed in this section used the uniform temperature objective with a semi-conjugate thermal analysis. In the semi-conjugate procedure, the optimization program was started with a CFD

analysis of the turbine cascade using an unstructured compressible turbulent Navier-Stokes solver (Han and Liu, 1997) and given an initial guess to the temperature, T_O, on the turbine blade surface. The CFD solver used the turbine inlet static temperature, T_{inlet}, inlet static pressure, p_{inlet}, back pressure, p_{exit}, and inlet Mach number, M_{inlet}, for its boundary conditions (see Table 1). Once converged, the flow-field analysis code computed turbulent heat fluxes, Q_O, that were applied as thermal flux boundary conditions directly to the BEM heat conduction analysis code. After converging on the non-linear boundary conditions of the coolant passages, new blade surface hot wall temperatures were computed by the BEM. Since this wall temperature variation was, in general, different from the wall temperatures specified to the hot gas flow-field analysis code, they were applied as boundary conditions again to the CFD code. The new CFD solution then returns heat fluxes that were again different from the ones that were used initially. This process was repeated several times until finally the heat fluxes converged. Thereafter, heat transfer coefficients, h_O, on the outer turbine airfoil boundary were computed from the converged hot surface temperatures and fluxes and the corresponding turbine inlet temperature, that is, $h_O = Q_O/(T_O - T_{inlet})$. This heat transfer coefficient variation was used and remained fixed for several optimization cycles.

Table 1. List of boundary conditions and constants for the uniform temperature optimization of a thermal barrier coated turbine blade.

p_{inlet}	588131 Pa
p_{exit}	134115 Pa
$\dot{m}$ (initial guess)	0.025 kg/s
Inlet Mach number	0.1772
T_{inlet} (initial guess)	1592.6
$k_{coating}$	1.0 W/m K

k_{metal}	30.0 W/m K
C (thermal barrier coating thickness)	0.1 mm
$\overline{T}$	1100 K
ε	0.1 mm
T_{max}	1250.0 K

Table 2. Geometric and cooling scheme design variables used for uniform temperature thermal optimization of an internally cooled turbine thermal barrier coated blade.

Design Variable	*Number*
Beta-Spline Coolant Wall Thickness	8
Strut Coordinates (2 per strut)	6
Strut Thickness (1 per strut)	3
Strut Filleting (2 per strut)	6
Wall Roughness (1 per passage)	4
Mass Flow Rate	1
Turbine Inlet Temperature	1

As the optimization algorithm ran, it modified the turbine inlet temperature. Once the new turbine inlet temperature was significantly different, the entire iterative procedure between the BEM and CFD was performed again. This global conjugate process was done only a small number of times during the course of the entire optimization.

Figure 2 illustrates the different variations of blade hot surface heat fluxes computed after subsequent iterations of the semi-conjugate procedure. In this figure, each intermediate flux (dT/dn) variation is

shown in dotted lines for the turbine inlet temperatures of Tinlet = 1487 K, 1562 K and 1441 K. The solid line shows the optimized flux at a turbine inlet temperature of 1510 K. The computed heat transfer coefficient distribution on the outer turbine airfoil is shown in Figure 3.

The constrained hybrid numerical optimization used the geometric and cooling scheme design variables listed in Table 2. The coolant wall roughness, coolant mass flow rate, and turbine inlet temperature were design variables. The total number of design variables was 29. A target temperature of the uniform temperature objective was 1100 K. The maximum temperature equality constraint was enforced during the entire optimization process. Implicit design sensitivity was used to compute the gradients of the objective and constraint functions. The thermal optimization algorithm began from the initial guess shown along with the flooded temperature contours computed by the BEM in Figure 4. The numerical heat conduction analysis of the initial guess to the geometry, turbine inlet temperature, coolant mass flow rate and wall roughness (see Table 1) predicted a maximum temperature of around 1160 K. The first thing that the constrained hybrid optimization

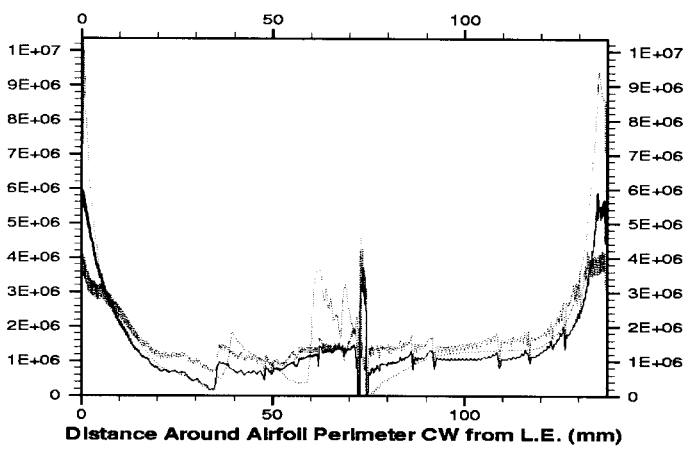

Figure 2. Fluxes (dT/dn in K/m) computed by the unstructured CFD flow solver on the surface of the cooled turbine thermal barrier coated blade for the semi-conjugate coupling procedure.

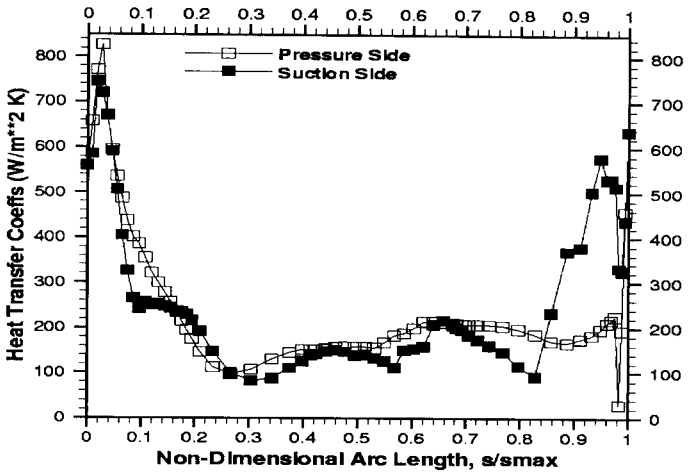

Figure 3. Heat transfer coefficient distribution predicted by the unstructured CFD on the outer turbine airfoil boundary.

program did was restore the design to the feasible equality constraint. That is, the coolant wall boundary conditions were modified using a gradient-based (DFP) minimization of the equality constraint function, $h_1(V_i)$, until the maximum temperature in the metal was equal to 1250 K (+/- 10 K). This required two sub-optimization cycles to initially restore the design to feasibility, and the new temperature contours are shown in Figure 5. The constrained hybrid optimizer did this many times during the course of the entire procedure, and each sub-optimization of an infeasible design (produced by DFP, GA, NM, or SA) required about 1-3 cycles to restore the constraint.

The constrained hybrid numerical optimization algorithm ran for less than 8 hours on Cray C-90 for 37 iterations. This problem required 997 computational heat conduction analyses and 5 CFD analyses in order to reach a converged solution. The optimization was started with the GA and ran for 12 iterations before switching automatically to the NM optimizer. The hybrid optimizer then switched back and forth to the SA algorithm when the NM failed after 3 iterations. The remainder of the optimization cycles (about 20 iterations) utilized all four

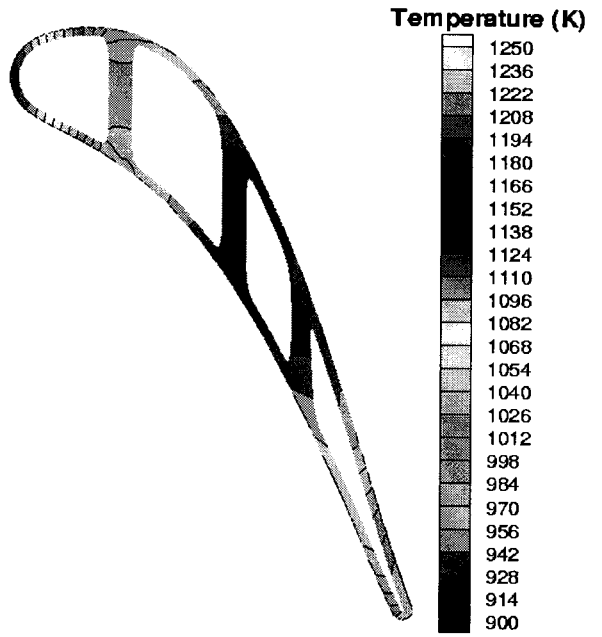

Figure 4. Temperature field computed by the BEM for the initial guess of an internally cooled and thermal barrier coated turbine blade.

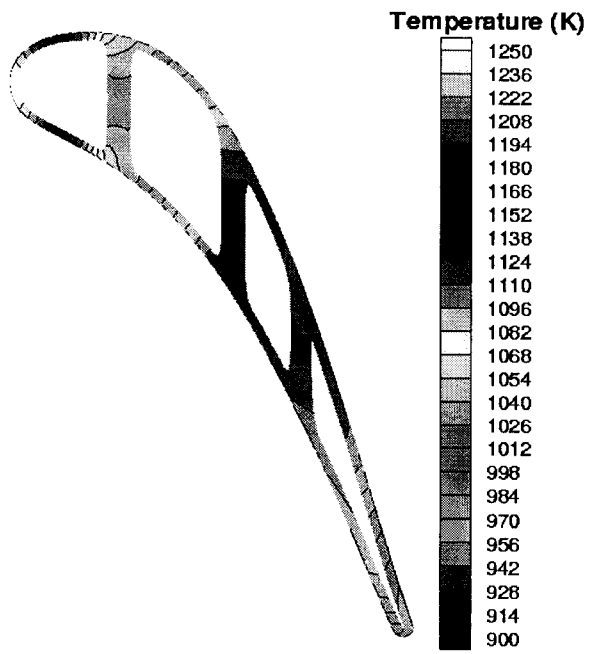

Figure 5. Temperature field computed by the BEM for the first feasible design of an internally cooled and thermal barrier coated turbine blade.

algorithms (DFP, GA, NM, and SA) until the program ended when all four algorithms failed to improve the objective function. The most significant modifications to the design occurred during the first 8 optimization cycles and the program only slightly modified the designs in the remaining cycles. The temperatures on the coating/metal interface boundary are shown in Figure 6.

One can see that the mean temperature in the blade rose significantly from about 950 K at the initial guess to 1100 K at the end of the optimized coolant passage design. Also shown here is the wall temperature variation after the first restoration to feasibility. This demonstrates a typical result of the uniform temperature field objective. The turbine inlet temperature did not consistently increase (Figure 7), although the coolant mass flow rate did reduce noticeably (Figure 8).

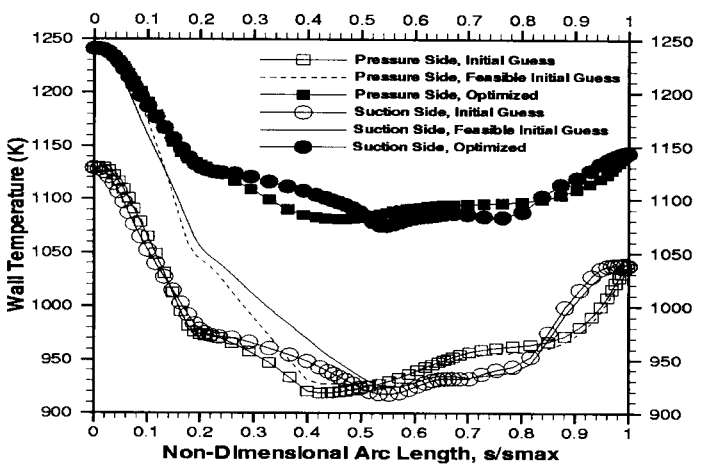

Figure 6. Wall temperature variation on coating/metal interface for the initial guess, first feasible, and optimized designs produced by the thermal optimization for uniform temperature.

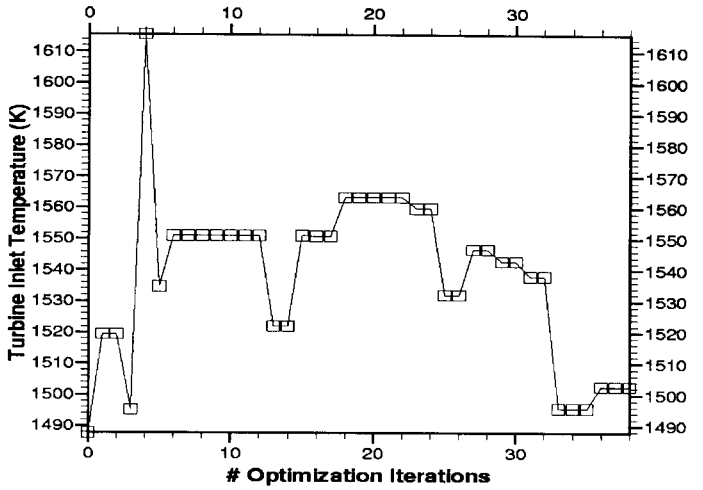

Figure 7. Evolution of the turbine inlet temperature for uniform temperature thermal optimization of an internally cooled and thermal barrier coated turbine blade.

The most undesirable features of this run were that the coolant heat transfer coefficient at the trailing edge coolant passage walls increased until it reached its maximum allowable value of 2400 W / m^2 K, while the bulk coolant temperatures rose to nearly the target temperature of 1100 K (see Figures 9 and 10).

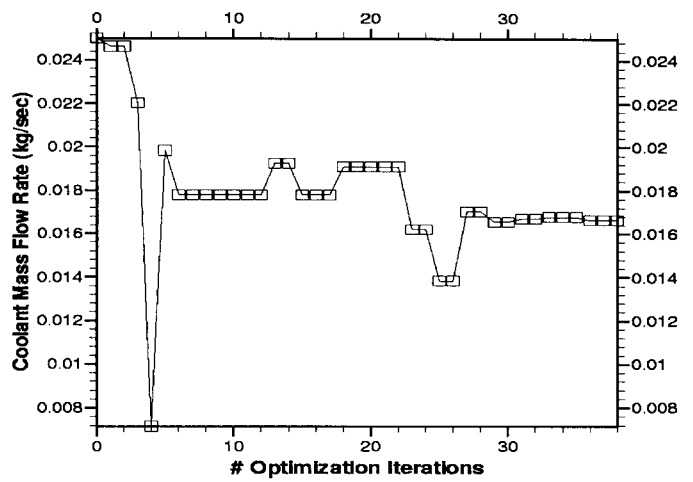

Figure 8. Evolution of the coolant mass flow rate for the uniform temperature thermal optimization of an internally cooled and thermal barrier coated turbine blade.

In order to produce these high heat transfer rates, the pressure losses in the coolant channels became very high requiring nearly the highest pressure available in the compressor.

Additional thermal optimization runs with the uniform temperature field objective were attempted using the mean temperature, $\overline{T}$, instead of a fixed target temperature. The result was a very uniform temperature field in the blade (Figure 11). This objective had an even more pronounced effect on the coolant heat transfer coefficients and bulk temperatures. They reached a minimum where the mean temperature and bulk coolant temperatures were as close as possible to the maximum temperature in the metal. The optimization algorithm accomplished this by increasing the coolant heat transfer coefficients as well as the coolant pressure and the coolant mass flow rate. Also, the turbine inlet temperature was decreased until it was nearly equal to the maximum temperature in the metal. It became apparent that the program was trying to make all temperatures everywhere equal to the maximum temperature, $\overline{T_{max}}$.

Although the uniform temperature objective did have some desirable features, it has been concluded that it does not satisfy the criterion established for internal coolant passage optimization.

5.2 Turbine Cooling Scheme Optimization for Minimum Coolant Ejection Temperature

The uniform temperature and heat flux extrema objectives were not entirely successful at producing internal blade geometry that would be considered economical or even physically realizable. The minimum heat flux objective tried to eliminate the coolant passages. The maximization of the net heat flux thinned the coolant walls and produced an extreme range of temperatures that questioned the validity of the use of heat transfer coefficients on the outer surface of the blade.

Therefore, another objective was tried by minimizing the coolant temperature at the very end of the coolant flow passage (the ejection slot at the blade trailing edge). Using the minimum coolant ejection temperature as the objective, the coolant flow passages are prevented from disappearing because, as they

are reduced in size, the speed of the coolant increases, thereby producing higher pressure losses that directly result in the increased temperature fed to the coolant flow passages.

From the opposite perspective, reduced heat transfer coefficients result in lower coolant pressure requirements. Thus, compressor bleed air can be extracted from lower compressor stages in which the air is cooler. The law of adiabatic heating during compression makes the inlet coolant temperature proportional to the compressor bleed air pressure. The quasi-one-dimensional flow (with heat addition and friction) analysis of the coolant fluid dynamics was coupled to the heat conduction in the turbine blade through the coolant wall heat flux. When the coolant ejection temperature is minimized, the coolant wall heat flux to the coolant is reduced via conservation of energy. This heat flux was found to be most sensitive to reductions in the heat convection coefficients.

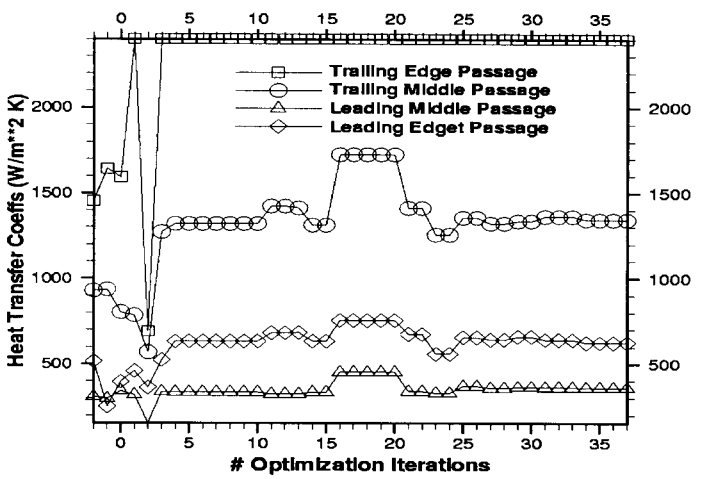

Figure 9. Evolution of coolant heat transfer coefficients for uniform temperature thermal optimization of an internally cooled and thermal barrier coated turbine blade.

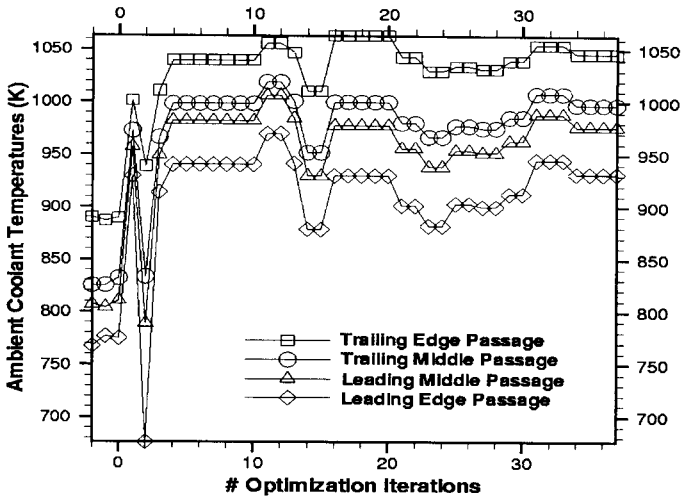

Figure 10. Evolution of the bulk coolant temperatures for the uniform temperature thermal optimization of an internally cooled and thermal barrier coated turbine blade.

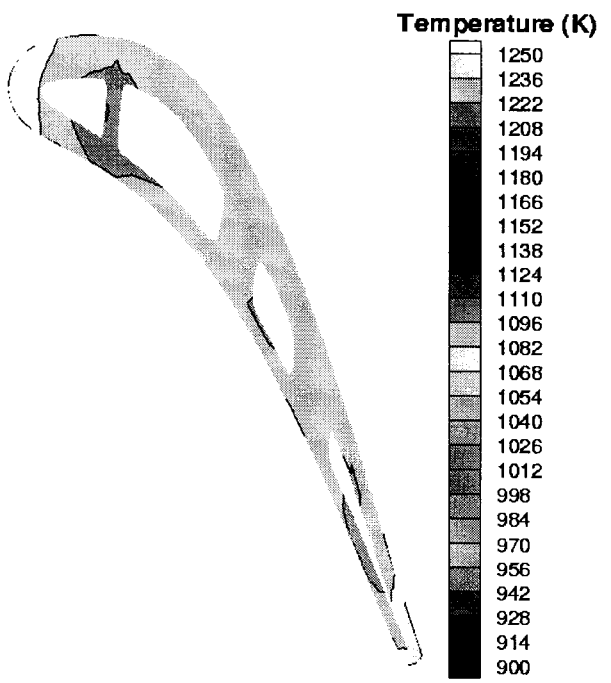

Figure 11. Temperature field computed by the BEM for the optimized design of an internally cooled and thermal barrier coated turbine blade.

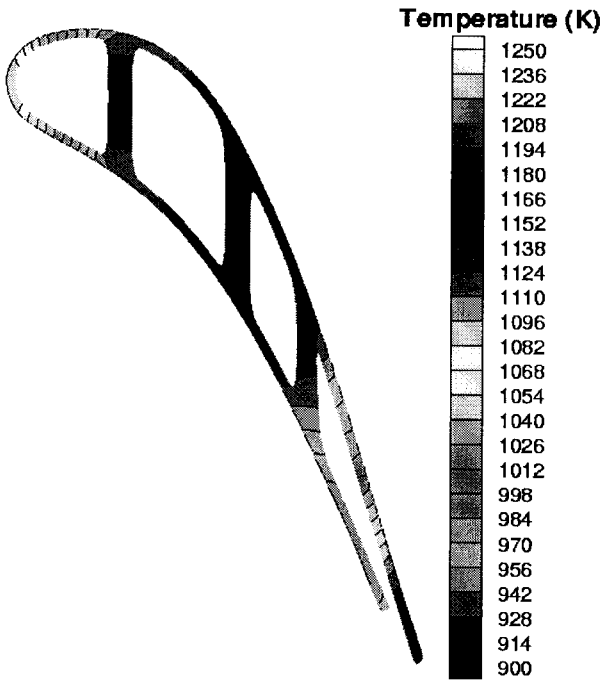

Figure 12. Temperature field computed by the BEM on the initial guess geometry used for the minimization of coolant ejection temperature.

Very low heat convection requirements might even allow the removal of heat transfer enhancements, such as, trip strips and impingement schemes, which would lead to a substantial reduction in turbine blade manufacturing costs.

In the following example, the trailing edge coolant passage was modeled with the addition of an ejection slot. This can be seen along with the temperature field computed on the initial guess geometry in Figure 12. Otherwise, the initial guess geometry and boundary conditions were the same as those found in Table 1, and the set of design variables was the same as in Table 2.

Two different minimizations of the coolant ejection temperature, T_{eject}, were performed; one with the maximum temperature equality constraint, $T_{max} = \overline{T_{max}}$, and the other with the inequality constraint $T_{max} < \overline{T_{max}}$. The design sensitivity gradients were calculated using finite differencing and the

optimization program was started with the DFP. The optimization with the equality constraint required 15 cycles and 794 objective function evaluations. The large number of function evaluations was because forward finite differencing was used to obtain the sensitivity gradients. After 4 optimization cycles, the program switched to the GA, switching finally to the NM in the 14th cycle.

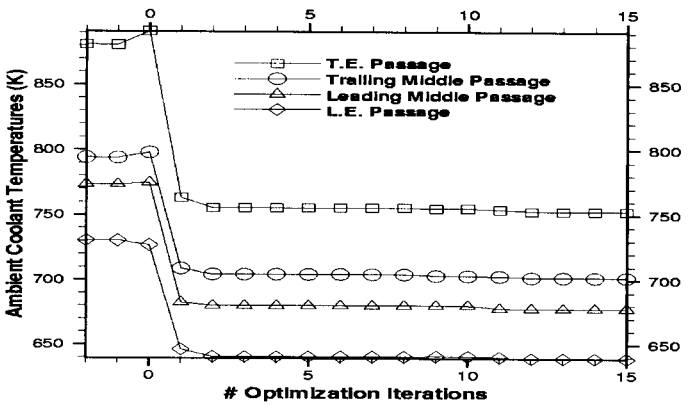

Figure 13. Evolution of bulk coolant temperatures for the minimization of coolant ejection temperature using the maximum temperature equality constraint.

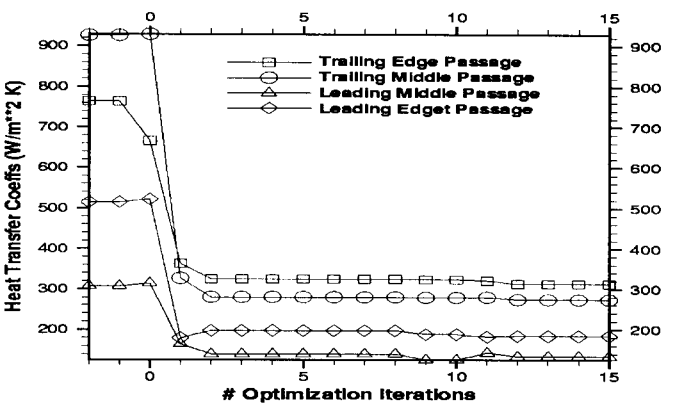

Figure 14. Evolution of coolant heat transfer coefficients for the minimization of coolant ejection temperature using the maximum temperature equality constraint.

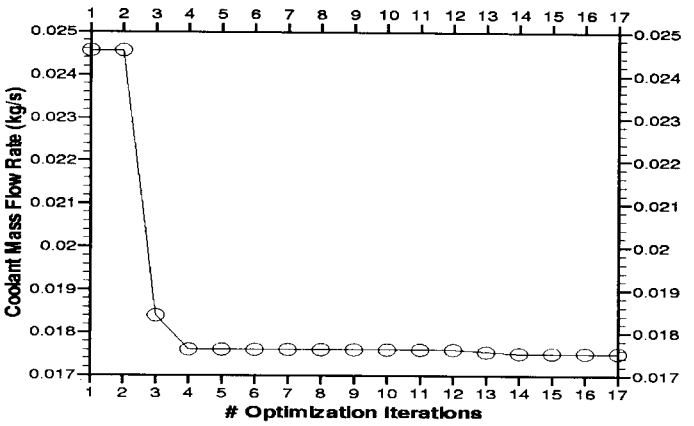

Figure 15. Evolution of coolant mass flow rate for the minimization of coolant ejection temperature using the maximum temperature equality constraint.

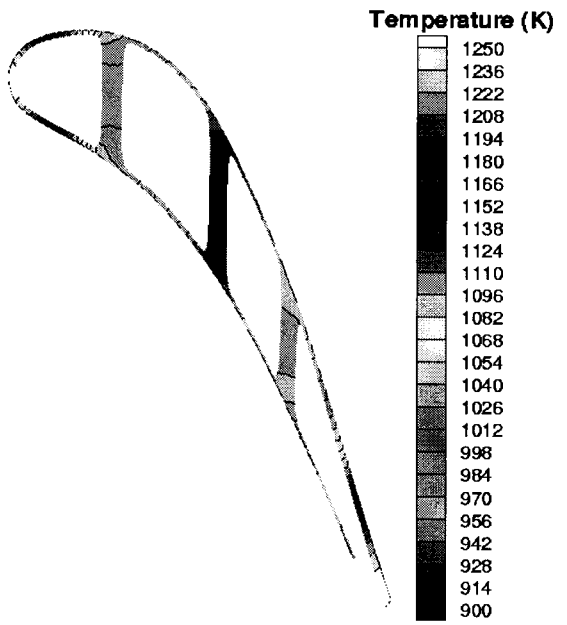

Figure 16. Temperature field computed by the BEM for minimized coolant ejection temperature design of an internally cooled turbine blade using the maximum temperature equality constraint.

Figure 13 shows how the bulk coolant temperatures were reduced during the optimization. The reduction in coolant temperatures also significantly reduced the pressure losses and the coolant heat transfer coefficients (Figure 14). The ultimate goal (reduction in the coolant mass flow rate) was achieved (Figure 15) by reducing the heat transfer coefficients and by making the passage walls thinner (Figure 16).

The turbine inlet temperature changed very little when the maximum temperature equality constraint was enforced with this objective. But, when the maximum temperature inequality constraint was enforced, the turbine inlet temperature was allowed to decrease from 1600 K down to 1340 K. The coolant mass flow rate was reduced even more dramatically (Figure 17). It is interesting to note that the optimization with the maximum temperature inequality constraint ran for more cycles (40), but required fewer objective function evaluations (521). This was because of the fewer number of gradients needed of the inequality constraint functions. That is, the equality constraint was always active, but the inequality constraint was only active when the maximum temperature in the blade was equal to or greater than the target maximum temperature, $\overline{T_{max}}$.

The final optimized configuration had extremely thin walls and struts (Figure 18) which were nearly at the lower limits enforced by the bounds on their design variables. This configuration is clearly unacceptable because of the reasonable doubts that such a thin walled blade could sustain the mechanical stresses.

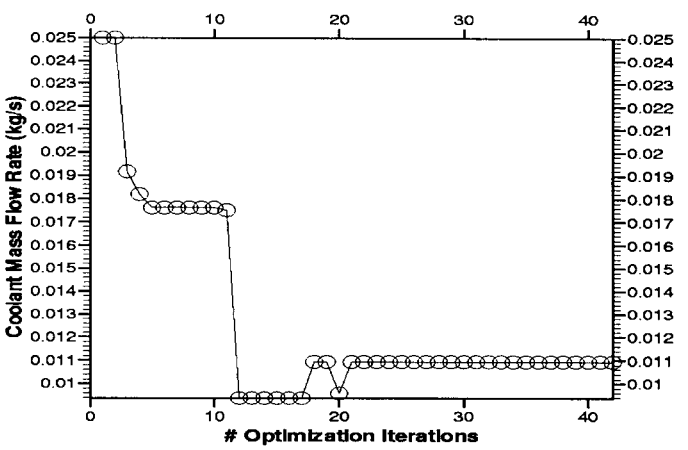

Figure 17. Evolution of coolant mass flow rate for the minimization of coolant ejection temperature using the maximum temperature inequality constraint function.

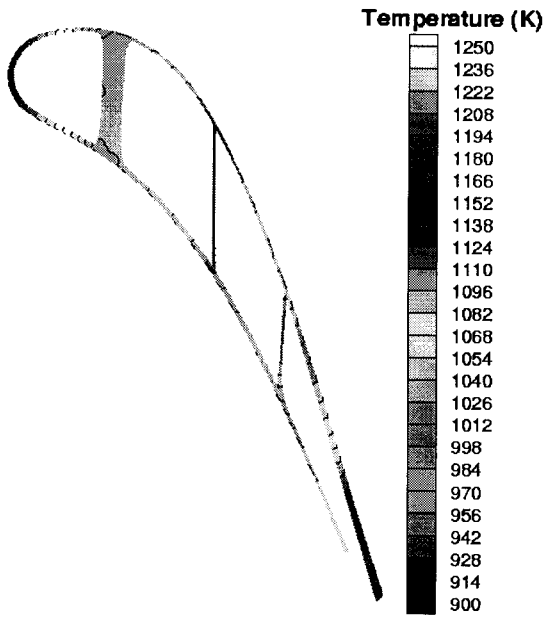

Figure 18. Temperature field computed by the BEM for minimized coolant ejection temperature design of an internally cooled turbine blade using the maximum temperature inequality constraint.

CONCLUSIONS

A preliminary design optimization tool has been developed for quasi-conjugate aero-thermal optimization of internally cooled turbine blades with or without thermal barrier coating and no film cooling. Lessons learned from this effort lead to the question, "Can we design a turbine cooling scheme that simultaneously increases the turbine inlet temperature and decreases the required coolant mass flow rate with a constraint of keeping the maximum temperature of the blade material below a specified limit?" This research introduced the possibility of using multi-disciplinary objective and constraint functions to achieve these goals simultaneously. Unfortunately, both of these quantities were used as

design variables in our coolant flow passage optimization procedure. For this reason, they could not be extremized explicitly.

Several alternative objectives were formulated. The uniform temperature objective was effective at reducing the temperature gradients in the blade, but it did not always produce effective coolant flow passage designs.

Extremization of the integrated heat flux into the blade produced only the trivial results of reducing the sizes of the coolant passages (minimum integrated heat flux), or by making the coolant walls as thin as possible (maximum integrated heat flux).

The minimization of the coolant temperature at the ejection point, while enforcing the maximum temperature equality constraint, was successful. It decreased the required coolant mass flow rate and the required coolant heat transfer coefficients (thus coolant passage surface roughness and coolant pressure losses) for the test cases that were studied, while keeping the turbine inlet temperature almost unchanged.

But, when the minimization of the coolant temperature at the ejection point was performed while enforcing the maximum temperature inequality constraint, the results were unacceptable. Although the required coolant mass flow rate reduced significantly, the turbine inlet temperature also decreased significantly. Besides, the walls and the struts of the resulting blade were unacceptably thin.

The complex multi-component nature of this design problem seems to force the designer to decide whether to maximize the turbine inlet temperature or minimize the coolant mass flow rate. Any dual objective would require an automated decision making process which could involve weighting the objective functions or alternating between the objectives and the constraints.

ACKNOWLEDGMENTS

The authors are grateful for NASA-Penn State Space Propulsion Engineering Center Graduate Student Fellowship facilitated by Professor Charles Merkle, National Science Foundation Grants DMI-9522854 and DMI-9700040 monitored by Dr. George Hazelrigg, NASA Lewis Research Center Grant NAG3-

1995 facilitated by Dr. John Lytle, and supervised by Dr. Kestutis Civinskas, the ALCOA Foundation Faculty Research Fellowship facilitated by Dr. Yimin Ruan, and for Lockheed Martin Skunk Works grant monitored by Mr. Thomas Oatway.

REFERENCES

Arpaci, V. S., 1966, *Conduction Heat Transfer*, Addison-Wesley Publishing Company, Reading, MA.

Barsky, B. A., 1988, *Computer Graphics and Geometric Modeling Using Beta-Splines*, Springer-Verlag, Berlin, Germany.

Brebbia, C. A., 1978, *The Boundary Element Method for Engineers,* John Wiley & Sons, New York.

Dulikravich, G. S. and Martin, T. J., 1996, "Inverse Shape and Boundary Condition Problems and Optimization in Heat Conduction", Chapter no. 10 in *Advances in Numerical Heat Transfer - Volume I* (editors: W. J. Minkowycz and E. M. Sparrow), Taylor and Francis, pp. 381-426.

Dulikravich, G. S., Martin, T. J., Dennis, B. H., Lee, E.-S. and Han, Z.-X., 1998, "Aero-Thermo-Structural Design Optimization of Cooled Turbine Blades," *AGARD - AVT Propulsion and Power Systems Symposium on Design Principles and Methods for Aircraft Gas Turbine Engines*, Editor: G. Meauze, Toulouse, France, May 11-15, 1998.

Dulikravich, G. S., Martin, T. J. and Han, Z.-X., 1998, "Aero-Thermal Optimization of Internally Cooled Turbine Blades," *Fourth ECCOMAS Computational Fluid Dynamics Conference,* Editors: K. Papailiou, D. Tsahalis, J. Periaux, D. Knoerzer, Athens, Greece, September 7-11, 1998, Vol. 2, pp.158-161, John Wiley & Sons, NY.

Foster, N. F. and Dulikravich, G. S., 1997, "Three-Dimensional Aerodynamic Shape Optimization using Genetic Evolution and Gradient Search Algorithms", *AIAA Journal of Spacecraft and Rockets*, Vol. 33, No. 3, pp. 33-33.

Goldberg, D. E., 1989, *Genetic Algorithms in Search, Optimization and Machine Learning*, Addison-Wesley.

Hafka, R. T. and Gurdal, Z., 1992, *Elements of Structural Optimization*, 3rd edition, Kluwer Academic Publ., Boston, MA.

Hafka, R. T. and Malkus, D. S., 1981, "Calculation of Sensitivity Derivatives in Thermal Problems by Finite Differences," *Int. Journal Numerical Methods in Engineering.*, Vol. 17, pp. 1811-21.

Han, Z. X. and Liu, Z. J., November 1997, "Numerical Calculation of 2-D Inviscid Flow-Fields on Unstructured Grids", *Journal of Engineering Thermophysics*, Vol. 18, No.6.

He, M., Kassab, A. J., Bishop, A. J., and Minardi, A., 1995, "An Iterative FDM/BEM Method for the Conjugate Heat Transfer Problem - Parallel Plate Channel With Constant Outside Temperature," *Engineering Analysis with Boundary Elements*, No. 15, pp. 43-50.

Holman, J. P., 1981, *Heat Transfer*, Fifth Edition, McGraw Hill Book Company.

Martin, T. J. and Dulikravich, G. S., 1997, "Aero-Thermal Analysis and Optimization of Internally Cooled Turbine Blades", *XIII International Symposium on Airbreathing Engines (XIII ISABE)*, Chattanooga, TN, Sept. 8-12, 1997.

Mochizuki, S., Takamura, J., Yamawaki, S., and Yang, W. J., 1994, "Heat Transfer in Serpentine Flow Passages With Rotation," *Journal of Turbomachinery*, Vol. 116, pp. 133-140.

Press, W. H, Teukolsky, S. A., Vetterling, W. T. and Flannery, B. P., 1986, *Numerical Recipes in FORTRAN, The Art of Scientific Computing*, 2nd Edition, Cambridge University Press, Cambridge.

Stephens, M. A. and Shih, T. I.-P., June 1997, "Computation of Compressible Flow and Heat Transfer in a Rotating Duct with Inclined Ribs and a 180-Degree Bend", ASME paper 97-GT-192, Orlando, Florida.

White, F. M., 1994, *Fluid Mechanics*, Third Edition, McGraw-Hill Book Company, New York.

White, F. M., 1988, *Heat and Mass Transfer*, Addison-Wesley, Reading, MA.

White, F. M., 1974, *Viscous Fluid Flow*, McGraw-Hill Book Company, New York.